Journal of the Physical Society of Japan
Vol. 69, No. 12, December, 2000, pp. 4095-4106

Two-Dimensional Spectroscopy for Harmonic Vibrational Modes with Nonlinear System-Bath Interactions. II. Gaussian-Markovian Case

Yoshitaka TANIMURA* and Thomas STEFFEN[1]

Institute for Molecular Science and the Graduate University for Advanced Studies, Myodaiji, Okazaki, Aichi 444-8585
[1] *Ultrafast Laser and Spectroscopy Laboratory, Department of Chemical Physics, University of Groningen, Nijenborgh 4, 9747 AG Groningen, The Netherlands*

(Received July 3, 2000)

The relaxation processes in a quantum system nonlinearly coupled to a harmonic Gaussian-Markovian heat bath are investigated by the quantum Fokker-Planck equation in the hierarchy form. This model describes frequency fluctuations in the quantum system with an arbitrary correlation time and thus bridges the gap between the Brownian oscillator model and the stochastic model by Anderson and Kubo. The effects of the finite correlation time and the system-bath coupling strength are studied for a harmonic model system by numerically integrating the equation of motion. The one-time correlation function of the system coordinate, which is measured in conventional Raman and infrared absorption experiments, already reflects the inhomogeneous character of the relaxation process. The finite correlation time of the frequency fluctuations, however, is directly evident only in the two- and three-time correlation function as probed by multidimensional spectroscopic techniques such as the Raman echo and the fifth-order 2D Raman experiment.

KEYWORDS: 2D spectroscopy, Gaussian-Markovian, nonlinear system-bath interaction

§1. Introduction

The interactions between the reacting molecules and their neighbors determine the reaction path and dynamics of virtually all chemical reactions in condensed phase systems. In order to better understand the basic chemical and biological processes various theoretical approaches such as *ab initio* calculations and molecular dynamics simulations have been taken. Optical spectroscopy is a very popular technique to study these processes experimentally: The position, width and shape of vibrational and vibronic resonances directly reflect the strength and dynamics of the most important molecular interactions. In spectroscopy, two relaxation processes are often distinguished:[1-3] Energy relaxation is the process in which the excited electronic or vibrational states of a probe molecule (the *system*) return to the ground state by transferring the energy difference to the environmental molecules (the *heat bath*). Phase relaxation is caused by fluctuations of molecular energy levels, which destroys the phase coherence without energy dissipation. The lifetime of the excited state has then no meaning and is considered infinitely long.

Theoretically, relaxation effects have been studied extensively by using a system-bath model,[2-4] such as the spin-Boson system, which consists of a two-level molecular system coupled to a harmonic oscillator bath. The spin-Boson Hamiltonian is expressed as[5]

$$H = \frac{1}{2}\hbar\omega_0 a^+ a + \frac{1}{2}F(a^+, a)\sum_j c_j(b_j + b_j^+) + \sum_j \left(\frac{1}{2}\hbar\omega_j b_j^+ b_j\right), \quad (1)$$

where a and a^+ are the creation and annihilation operators of the two-level system, b_j and b_j^+ are those of the jth bath oscillator. The interaction between the system and the bath is linear in the bath coordinates, but can be any function $F(a, a^+)$ of the system coordinate. The heat bath acts as noise source, which induces fluctuations in the two-level system through the system-bath interaction. The noise is characterized by the noise correlation function $f(t) = \int \mathrm{d}\omega J(\omega)\sin(\omega t)$, where $J(\omega) = \sum(c_j^2/\hbar\omega_j)\delta(\omega-\omega_j)$ is the spectral density of the bath. Usually, one assumes Gaussian-white noise, $f(t) = \kappa\delta(t)$ with $J(\omega) \propto \kappa\omega$,[6] or Gaussian-Markovian noise, $f(t) = \Delta^2\exp(-\gamma t)$ with $J(\omega) \propto \Delta^2\omega\gamma/(\gamma^2+\omega^2)$, in which γ corresponds to the inverse correlation time of the noise.[7,8]

One popular approach to study energy relaxation processes is using the optical Bloch equation.[1,6] This equation is obtained by assuming Gaussian-white noise with linear system-bath interaction $F = a + a^+$ and evoking the rotating wave approximation $(a + a^+)\sum c_j(b_j + b_j^+) \to \sum c_j(a^+ b_j + a b_j^+)$. These two terms describe resonant energy exchange between the two-level system and the heat bath. Since for a Gaussian-white noise heat bath the spectral distribution is continuous, i.e., $J(\omega) \propto \kappa\omega$, there is an infinite number of the bath oscillators with different frequencies in every frequency interval $\omega \pm \delta\omega$.

* E-mail: tanimura@ims.ac.jp

Thus, the energy transferred from the system to the bath does not return to the system in a finite time, yielding an effective energy relaxation of the system. The rate 2κ appearing in the Bloch equation corresponds to the population relaxation from the excited state to the ground state, which is analogous to $1/T_1$ in nuclear magnetic relaxation.

The phase relaxation can be taken into account by assuming fluctuations of the energy levels, which leads to the stochastic Liouville equation.[9] The random modulation of energy levels causes a phase loss of the initial coherence between the ground and the excited state, which can be incorporated into the spin-Boson Hamiltonian by setting $F = a^+a$. Such a term is found for a coupling that is linear in the bath coordinate and quadratic in the system coordinate, i.e., $Q^2 \sum c_j x_j \to (a+a^+)^2 \sum c_j(b_j+b_j^+)$ (SL model). In our previous paper (here after paper I)[10] we showed that in the limits of Gaussian-white noise and weak coupling this model describes phase relaxation, i.e., the T_2 process in NMR, see also the discussion above. In many cases, *e.g.*, molecular collisions or lattice vibrations, the Markovian approximation of completely uncorrelated fluctuations is valid. In liquids, however, where the motions of the bath molecules have similar time constants as the motions of the system, this approximation can break down and a more elaborated model is necessary, which accounts for the finite correlation of the system and the bath motions. Then the phase relaxation process cannot be characterized by a single decay constant $1/T_2$ anymore since here we consider a colored noise. The simplest example is a Gaussian-Markovian modulation defined by the noise correlation function $f(t) = \Delta^2 \exp(-\gamma t)$.[7,8]

To make this discussion more concrete, we discuss the effects of energy and phase relaxation upon linear absorption in a two-level system. We assume that the bath is in the high temperature equilibrium state; $\rho_{\rm B}^{\rm eq} = \exp(-\sum \beta\hbar\omega_j b_j^+ b_j/2)$, where β is the inverse temperature of the bath. If the two-level system is initially in the ground state, $|0\rangle\langle 0|$, then the linear absorption signal is calculated as[2]

$$I(t) = tr\{a^+(t)a|0\rangle\rho_{\rm B}^{\rm eq}\langle 0|\} = \exp[-{\rm i}\omega_0 - g(t)], \qquad (2)$$

where the line shape function $g(t)$ is expressed in the Gaussian-white (GW) case as

$$g_{\rm GW}(t) = \kappa t, \qquad (3)$$

and in the Gaussian-Markovian (GM) case as

$$g_{\rm GM}(t) = \frac{\Delta^2}{\gamma^2}(e^{-\gamma t} + \gamma t - 1). \qquad (4)$$

The Gaussian-Markovian case is characterized by two parameters, the inverse correlation time of the frequency fluctuations γ and the width of the frequency fluctuations Δ. In the fast modulation limit, $\gamma \gg \Delta$, the bath perturbs the energy levels so rapidly that the system cannot follow these motions. It experiences then an effective bath (motional narrowing) and the line shape function can be approximated by $g_{\rm GM}(t) = \gamma' t$ with $\gamma' \equiv \Delta^2/\gamma$, corresponding to a Lorentzian shape of the spectral line. This limit describes the phase relaxation described above. In the opposite case of slow modulation, $\gamma \ll \Delta$, the bath configuration is effectively static and the line shape function is $g_{\rm GM}(t) = \Delta^2 t^2/2$; the spectral line shape is then Gaussian. This is indeed identical with the case that the two-level molecules are distributed spatially with the Gaussian distribution function $S(\omega) = \exp[-\delta^2(\omega-\omega_0)^2]$. The linear absorption spectrum is expressed as

$$I_{\rm inhomo}(t) = \int {\rm d}\omega S(\omega) e^{{\rm i}\omega t} = e^{{\rm i}\omega_0 t - \Delta^2 t^2/2}, \qquad (5)$$

where we put $\Delta^2 = \delta^2/2$. This inhomogeneous broadening is found, *e.g.*, for molecules in the gas phase (Doppler broadening) or molecules at different sites in a crystal or glass matrix. When neither of the two limits applies and the inverse correlation time of the fluctuations is of the same order as the width of the fluctuations, the noise cannot be regarded as white and eq. (4) has to be used. The stochastic model has been applied to photon echoes,[2] resonant light scattering,[11] Raman echoes[12] and fifth-order Raman scattering.[13]

Although it surpasses the traditional descriptions in terms of population and phase relaxation rates, the stochastic model is still rather phenomenological in the sense that it does not involve a detailed microscopic description of the system and the bath. In particular, it is independent of the bath temperature and the shape of the system potential. The Brownian oscillator model is a more microscopic approach to the dynamics of a system with a potential $U(Q)$, which is in contact with a distribution of bath oscillators. The Hamiltonian is then given by:[14]

$$H = \frac{P^2}{2M} + U(Q) + \sum_{j=1}^{N}\left[\frac{p_j^2}{2m_j} + \frac{m_j\omega_j^2}{2}\left(x_j - \frac{F_j(Q)}{m_j\omega_j^2}\right)^2\right]. \qquad (6)$$

Here, Q, P, and M denote the effective coordinate, conjugated momentum, and mass of the molecular system. The coordinate, conjugated momentum, mass and frequency of the jth bath oscillator are given by x_j, p_j, m_j and ω_j, respectively. The coupling between the system and the jth bath oscillator is controlled by the function $F_j(Q)$, which is related to the system-bath interaction via: $H_{\rm SB} = -\sum x_j F_j(Q)$.

In the simplest form of the Brownian oscillator model, the interaction is also linear in the system coordinate, $-\sum c_j x_j Q$ (the LL interaction). Since the coordinates can be expressed in terms of the creation and annihilation operators, a and a^+, and b_j and b_j^+, the interaction is rewritten as $(a+a^+)\sum c_j(b_j+b_j^+)$. In the rotating wave approximation, this is expressed as $\sum c_j(ab_j^+ + a^+b_j)$ implying that the LL model describes the energy relaxation (the T_1 relaxation process), besides the off-resonant terms, ab and a^+b^+. The pure phase relaxation, however, cannot be described by the LL model, even if we consider a Gaussian-Markovian modulation, since the LL interaction causes just dissipation and no frequency fluctuation.

In order to introduce pure dephasing due to level fluctuations, one has to consider the square-liner interaction (the SL model) in the Hamiltonian eq. (6) defined by $F_j(Q) = g_j Q^2/2$, where g_j is the coupling constant.[15] One can regard this interaction as a part of the total system-bath interaction expressed in the general form as $H_{\rm SB} = (Q + aQ^2 + \ldots)\sum(c_j x_j + c'_j x_j^2 + \ldots)$. Note that in spectroscopy the interaction between the modes of the form $Q^2 x$ is known as Fermi resonance. This interaction causes frequency modulations of the system, since the instantaneous frequency of the molecular oscillator is expressed as $\delta\omega(t) = \sqrt{\omega_0^2 + \sum g_j x_j(t)/M}$ for a harmonic potential $U(Q) = M\omega_0^2 Q^2/2$. Note that the relaxation in this model is, however, not completely equivalent to the pure dephasing, since in addition to $(aa^+ + a^+a)\sum g_j(b_j + b_j^+)$, this interaction includes higher-order population relaxation described by $(a^+a^+ + aa)\sum g_j(b_j + b_j^+)$. These effects were discussed for Gaussian-white noise in paper I.

As discussed for the two-level system, it is important to take into account the correlation of the noise to study memory effects. In the SL model the bath dynamics - and hence the system-bath correlation - is described by the spectral density

$$J_{SL}(\omega) = \sum_{j=1}^{N} \frac{g_j^2}{8m_j\omega_j}\delta(\omega - \omega_j). \tag{7}$$

Such distribution can be evaluated computationally based upon the molecular dynamics simulation.[16] In the previous paper, we discussed the Gaussian-white noise case, $J_{SL}(\omega) = M\zeta_{SL}\omega$, which corresponds to the homogeneous limit of the stochastic two-level model. In this paper, we consider a more general distribution function:[7, 8, 17-20]

$$J_{SL}(\omega) = M\zeta_{SL}\frac{\gamma^2\omega}{\gamma^2 + \omega^2}, \tag{8}$$

corresponding to an exponentially decaying correlation function $f(t) \propto \exp[-\gamma t]$. This distribution can represent an inhomogeneous distribution in the slow modulation limit, $\gamma \ll \omega_0$, where ω_0 is the characteristic frequency of the potential in the harmonic approximation, and reduces to the Gaussian-white case (paper I) in the fast modulation limit, $\gamma \gg \omega_0$, i.e. $J(\omega) = M\zeta_{SL}\omega$. In the previous paper I, we have calculated the seventh-order off-resonant Raman signal to compare it with the result from the stochastic Raman echo theory, which predicts an echo peak for inhomogeneously distributed two-level modes.[12] We showed that the SL model with a Gaussian-white bath does not have any echo like signal, since it corresponds to the homogeneous case. In the present paper, we demonstrate that this signal does show an echo for the exponentially correlated Gaussian-Markovian noise. We will also show that fifth-order 2D spectroscopies, which are of great interest both theoretically[21-46] and experimentally,[47-61] are sensitive to the correlation time of the noise.

In §2 the quantum Fokker-Planck equation for Gaussian-Markovian noise with nonlinear system-bath coupling is presented. A derivation of this equation is given in the appendix. The third-, fifth-, and seventh-order Raman response function, which is equivalent to the first-, second-, and third-order IR response is presented in §3 for purely inhomogeneous broadening; in §4 these results are compared to the results for a Gaussian-Markovian frequency fluctuation obtained by the hierarchical quantal Fokker-Planck approach. Section 5 is devoted to concluding remarks.

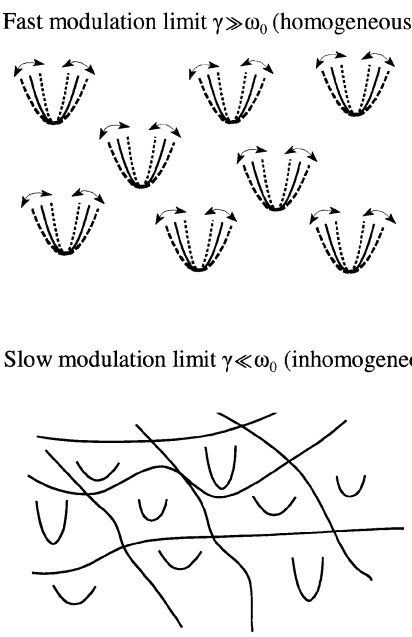

Fig. 1. Schematic view of homogeneous and inhomogeneous distribution of harmonic oscillators.

§2. The Gaussian-Markovian Quantum Fokker-Planck Equation for Nonlinear System-Bath Interaction

The Fokker-Planck equation was originally classical and for white noise.[62] Later, Caldeira and Leggett derived the quantum version from the system-bath Hamiltonian with LL interaction $F_j(Q) = c_j Q$ using the Feynman-Vernon influence functional formalism.[63] They assumed Ohmic dissipation $J_{\rm LL}(\omega) \propto \zeta\omega$, but later Tanimura and Wolynes derived the quantum Fokker-Planck equation in the tridiagonal hierarchy form for Gaussian-Markovian noise by assuming $J_{\rm LL}(\omega) \propto \zeta\omega\gamma^2/(\gamma^2 + \omega^2)$ and $\beta\hbar\gamma \ll 1$.[17-20] The equation of motion has then a similar structure as Kubo's stochastic Liouville equation.[9] The Fokker-Planck equation for arbitrary colored noise has also been studied.[64-66] All of these studies are, however, limited to LL coupling. In the previous paper, we derived the quantum Fokker-Planck equation for SL coupling and Gaussian-white noise by considering the Hamiltonian eq. (6) with coupling $F_j(Q) = g_j Q^2/2$.[10] In this study, we generalize it to Gaussian-Markovian noise. For the derivation of the Gaussian-Markovian Fokker-Planck equation in the SL model, which is given in the Appendix, one has to assume the spectral density eq. (8) and a high temperature bath $\beta\hbar\gamma \ll 1$. In the hierarchy form it can be expressed as:

$$\frac{\partial}{\partial t}W^{(0)}(P,R;t) = -\mathcal{L}_S W^{(0)}(P,R;t) + 2R\frac{\partial}{\partial P}W^{(1)}(P,R;t), \tag{9}$$

$$\frac{\partial}{\partial t}W^{(1)}(P,R;t) = -(\mathcal{L}_S+\gamma)W^{(1)}(P,R;t) + 2R\frac{\partial}{\partial P}W^{(2)}(P,R;t) + 2\zeta_{SL}\gamma\left[R\left(P+\frac{M}{\beta}\frac{\partial}{\partial P}\right)+\frac{\hbar^2}{4}\frac{\partial^2}{\partial P\partial R}\right]W^{(0)}(P,R;t), \tag{10}$$

and

$$\frac{\partial}{\partial t}W^{(n)}(P,R;t) = -(\mathcal{L}_S+n\gamma)W^{(n)}(P,R;t) + 2R\frac{\partial}{\partial P}W^{(n+1)}(P,R;t) + n2\zeta_{SL}\gamma\left[R\left(P+\frac{M}{\beta}\frac{\partial}{\partial P}\right)+\frac{\hbar^2}{4}\frac{\partial^2}{\partial P\partial R}\right]W^{(n-1)}(P,R;t), \tag{11}$$

where the quantal Liouvillian is expressed by the Fourier representation of the potential, which is convenient for numerical calculations:

$$-\mathcal{L}_S W(P,R;t) \equiv -\frac{P}{m}\frac{\partial}{\partial R}W(P,R;t) - \frac{1}{\hbar}\int\frac{\mathrm{d}P'}{2\pi\hbar}V(P-P',R)W(P',R;t), \tag{12}$$

with

$$V(P,R) = 2\int_0^\infty \mathrm{d}r\,\sin(Pr/\hbar)[U(R+r/2)-U(R-r/2)]. \tag{13}$$

The definition of hierarchy elements $W^{(n)}(P,R)$ is given in the Appendix. The equation of motion is derived by calculating the time derivative of these hierarchy elements. Physically, one can think of this hierarchy of equations as dealing with a set of Wigner functions, modeling the states of the system with various numbers of quanta exchanged between the system and the bath. In this formulation, $W^{(0)}$ includes all orders of the system-bath interaction; it is the exact solution for the Hamiltonian eq. (6) with the Gaussian-Markovian distribution eq. (8). Then $W^{(1)}$, $W^{(2)}$, ..., $W^{(n)}$ describe the distribution functions with a smaller set of the system-bath interactions, corresponding to the complete set of the system-bath interactions minus 1st, 2nd, ..., nth order of the system-bath interaction, respectively. Thus, this formulation takes the opposite direction to the conventional perturbation approaches, where the 0th member does not include any system-bath interaction, then the first, second, third, etc., members gradually take into account the higher-order interactions and approach the exact solution. We shall be interested only in the 0th member of the hierarchy, $W^{(0)}$, which is identical to the original Wigner distribution W. The other elements $n \neq 0$ are not directly related to any physical observable and are introduced for computational purposes only. At large $n = N \gg \omega_0/\gamma$ the inclusion of even more system-bath interactions does not yield any significant change anymore. The above hierarchy can then be terminated by

$$\frac{\partial}{\partial t}W^{(N)}(P,R;t) = -(\mathcal{L}_S+N\gamma)W^{(N)}(P,R;t) + \Gamma_{SL}W^{(N)}(P,R;t) + N2\zeta_{SL}\gamma\left[R\left(P+\frac{M}{\beta}\frac{\partial}{\partial P}\right)+\frac{\hbar^2}{4}\frac{\partial^2}{\partial P\partial R}\right]W^{(N-1)}(P,R;t), \tag{14}$$

where Γ_{SL} is the damping operator in the Gaussian-white case (see paper I):

$$\Gamma_{SL} = 4R^2\zeta_{SL}\frac{\partial}{\partial P}\left(P+\frac{M}{\beta}\frac{\partial}{\partial P}\right) + R\zeta_{SL}\hbar^2\frac{\partial^3}{\partial^2 P\partial R}. \tag{15}$$

The depth of the hierarchy N, i.e., the number of Wigner functions $W^{(n)}$, can be estimated from numerical simulations and should fulfill $N\gamma > 4\omega_0$ and $N\gamma > 4\zeta$. The error caused by the cutoff is easily checked by changing N. Using this hierarchal structure, we may deal with strong system-bath interactions in addition to the finite correlation time of the noise. In the white noise limit, $\gamma \gg \omega_0$, we may terminate the hierarchy of eqs. (9)–(14) by setting $N = 0$, obtaining the quantum Fokker-Planck equation for a Gaussian-white noise bath:

$$\frac{\partial}{\partial t}W(P,R;t) = -\mathcal{L}_S W(P,R;t) + \Gamma_{SL}W(P,R;t), \tag{16}$$

which agrees with the equation derived in paper I. Since we assumed $\beta\hbar\gamma \ll 1$, the temperature requirement in the Gaussian-white case is more stringent than in the Gaussian-Markovian case.

The physical observable in optical measurements can be expressed by the multi-time correlation function of polarizability or dipole moment. In vibrational spectroscopy, the optical responses of resonant IR and Raman are formally identical besides the fact that the Nth-order IR spectroscopy corresponds to the $(2N+1)$th-order Raman spectroscopy as shown in paper I.[10] For off-resonant excitation, the response functions are expressed in terms of the polarizability $\alpha(Q)$ as[21,25,26]

$$R^{(3)}(T_1) = \frac{i}{\hbar}tr\{[\alpha(T_1),\alpha(0)]\rho_g\}, \tag{17}$$

$$R^{(5)}(T_2,T_1) = -\frac{1}{\hbar^2} tr\{[[\alpha(T_1+T_2,\alpha(T_1)],\alpha(0)]\rho_g\}, \tag{18}$$

and

$$R^{(7)}(T_3,T_2,T_1) = -\frac{i}{\hbar^3} tr\{[[[\alpha(T_1+T_2+T_3),\alpha(T_1+T_2)],\alpha(T_1)],\alpha(0)]\rho_g\}. \tag{19}$$

Here, ρ_g is the equilibrium distribution

$$\rho_g = \exp[-\beta H]/tr\{\exp[-\beta H]\}, \tag{20}$$

and $\alpha(\tau)$ is the Heisenberg representation of the polarizability operator $\alpha(Q)$:

$$\alpha(\tau) \equiv \exp\left(\frac{i}{\hbar}H\tau\right)\alpha(Q)\exp\left(-\frac{i}{\hbar}H\tau\right). \tag{21}$$

For resonant IR excitation, the polarizability $\alpha(Q)$ is replaced by the dipole moment $\mu(Q)$. In both cases, the polarizability and dipole moments are expanded in the molecular coordinate as $\alpha(Q) = \alpha_1 Q + \alpha_2 Q^2 \ldots$, or $\mu(Q) = \mu_1 Q + \mu_2 Q^2 \ldots$, and the two results are formally identical. Therefore, hereafter we do not distinguish between the Nth-order IR and $(2N+1)$th order Raman processes and present only the results for Raman spectroscopy.

§3. Optical Response of the Pure Inhomogeneous Model

Before discussing the results for the Gaussian-Markovian model, in particular the role of the finite correlation time, it is instructive to discuss the response of a set of purely inhomogeneously broadened oscillators to explain the underlying physics in the higher-order optical processes. This is identical with the slow modulation limit discussed in §1, where the frequency of the harmonic oscillators are distributed with the distribution function $S(\omega)$ (Fig. 1(b)). As shown in ref. 21, the third-, fifth-, and seventh-order signals can be expressed as

$$R^{(3)}_{\rm inhomo}(T_1) = \frac{\alpha_1^2}{2M}\int d\omega \frac{S(\omega)}{\omega}\sin(\omega T_1), \tag{22}$$

$$R^{(5)}_{\rm inhomo}(T_2,T_1) = \frac{\alpha_1^2\alpha_2}{4M^2}\int d\omega \frac{S(\omega)}{\omega^2}\sin(\omega T_2)[\sin(\omega T_1)+\sin(\omega(T_1+T_2))], \tag{23}$$

$$R^{(7)}_{\rm inhomo}(T_3,0,T_1) = \frac{\alpha_1^2\alpha_2^2}{4M^3}\int d\omega \frac{S(\omega)}{\omega^3}\sin(\omega T_1)[\sin(\omega T_3)]^2. \tag{24}$$

In Fig. 2, we plot the third-, fifth- and seventh-order signals for $S(\omega) = \exp[-\delta^2(\omega-\omega_0)^2]$. The Gaussian distribution function is chosen because of the central limit theorem and, moreover, it is the static limit of the stochastic model. Figure 2(a) presents the imaginary part of the Fourier transformation of the third-order response function, $\mathrm{Im}\{R^{(3)}(\omega)\} \equiv \mathrm{Im}\{\int dT_1 \exp[i\omega T_1]R^{(3)}(T_1)\} = S(\omega)/\omega$ for $\delta = 2/\omega_0$ (short dashed line), $3/\omega_0$ (solid line) and $5/\omega_0$ (dotted line), where $\omega_0 = 38.7\,\mathrm{cm}^{-1}$ ($1/\omega_0 = 861\,\mathrm{fs}$) which is a typical value for low-frequency intermolecular motions and which has been used in a previous study of a Morse potential.[25] For small inhomogeneity $\delta = 5/\omega_0$ and $3/\omega_0$, the spectrum is Gaussian. The peak shifts to the red and becomes broader as δ decreases. For large inhomogeneity ($\delta = 2/\omega_0$), the line shape becomes bimodal: In addition to a broad feature around ω_0 there is a (nearly) Lorentzian peak close to zero frequency. This is because, in the large inhomogeneity case, the low frequency oscillators can contribute to the signal due to the large distribution. Their contribution to the signals are proportional to t, since $\sin(\omega t)/\omega t \to 1$ for $\omega t \ll 1$, causes the low frequency peak in frequency domain.

Figure 2(b) shows the fifth-order two-dimensional (2D) Raman signal $I^{(5)}(T_1,T_2) = R^{(5)}(T_2,T_1)$ for $\delta = 3/\omega_0$. The dashed lines represent the negative part of the signal. This signal has two prominent features: (i) a peak along T_2 for small T_1 and (ii) a peak along the diagonal at $T_1 = T_2$. Such directions are the stationary points of the response function, as we can easily see from eq. (23) by transforming the trigonometric functions in the response function into $\cos(\omega T_1)$ and $\cos[\omega(T_1-T_2)]$. The origin of these two peaks was discussed in ref. 27: The first peak involves a coherent state during the (short) first propagation time and a population during the second propagation time. Since the latter state is not affected by pure dephasing we find a plateau. The second peak along the diagonal is due to an inversion of the phase coherence leading to a vibrational echo. Figure 2(c) presents the seventh-order 2D Raman signal $I^{(7)}(T_1,T_3) = R^{(7)}(T_3,0,T_1)$ for $\delta = 3/\omega_0$. The stationary point of the response function is now $T_1 = 2T_3$ as can be seen from eq. (24) with transforming its trigonometric functions. Figures 2(b′) and 2(c′) illustrate the same result as Figs. 2(b) and 2(c) but in the frequency domain ($R^{(5)}(\omega_1,\omega_2) = |\int dT_1 \int dT_2 \exp[i\omega_1 T_1 + i\omega_2 T_2]R^{(5)}(T_2,T_1)|$ and $R^{(7)}(\omega_1,\omega_3) = |\int dT_1 \int dT_3 \exp[i\omega_1 T_1 + i\omega_3 T_3]R^{(7)}(T_3,0,T_1)|$). The peak along $T_1 = 0$ and $T_1 = T_2$ in Fig. 2(b) and $T_1 = 2T_3$ in Fig. 2(c) correspond to the spectral peaks along $\omega_2 = 0$ and $\omega_1 = -\omega_2$, and $\omega_1 = -2\omega_3$, respectively. In the frequency domain representation the line narrowing character of the 2D spectroscopies is clearly evident: The "length" of the peaks at $\omega_1 = -\omega_2$ and $\omega_1 = -2\omega_3$, i.e., the range of values ω_1 is a direct image of the distribution function $S(\omega)$. The "width" of the peaks, i.e., the range of values $\omega_{2(3)}$ for a given ω_1 which almost fulfill $\omega_1 = -\omega_2$ and $\omega_1 = -2\omega_3$, is a measure for the homogeneity of the system. In our simulation of purely inhomogeneous broadening the width is solely determined by the finite size of $S(\omega)$. Note that the peaks at $\omega_1 = \omega_2$ in Fig. 2(b′) are very small since the corresponding term

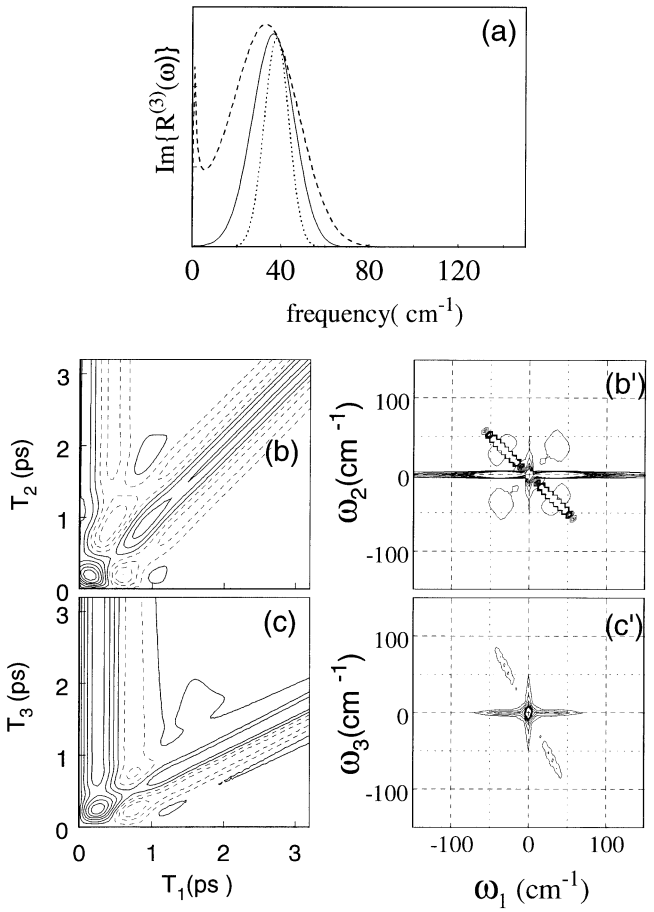

Fig. 2. The third-, fifth-, and seventh-order response for pure inhomogeneous case calculated from eqs. (22)–(24). (a) presents the third-order spectrum for $2/\omega_0$ (short dashed line), $3/\omega_0$ (solid line) and $5/\omega_0$ (dotted line), where $\omega_0 = 38.7\,\mathrm{cm}^{-1}$. (b) and (c) present the fifth- and seventh-order two-dimensional Raman signal, $I^{(5)}(T_1, T_2) = R^{(5)}(T_2, T_1)$ and $I^{(7)}(T_1, T_3) = R^{(7)}(T_3, 0, T_1)$ for $\delta = 3/\omega_0$. 2(b′) and 2(c′) illustrate the same result as 2(b) and 2(c) but in the frequency domain.

$\cos[\omega(T_1 + T_2)]$ does not rephase.

One may expect that the SL model with Gaussian-Markovian noise reduces to the above results in the slow modulation limit analogous to the two-level case. This is not always true in the higher-order optical processes as will be shown in the following sections.

§4. Optical Response of the SL Model with Gaussian-Markovian Modulation

In this Section we present the third-, fifth- and seventh-order Raman signals in the SL model for Gaussian-Markovian noise. For the calculation of the optical response upon multiple system-light interactions, we have first to generate the initial equilibrium state. This phase space distribution is obtained by integrating the equation of motion from time $t = -t_i$ to $t = 0$ with the temporally initial condition,

$$W^{(0)}(P, R; -t_i) = \exp[-\beta(P^2/2M + U(R))],$$
$$W^{(n)}(P, R; -t_i) = 0. \qquad (25)$$

Note that eq. (25) is the equilibrium state of the *uncoupled* system, but it is not the equilibrium state of the total system *and* the bath, since it neglects the interaction between the system and the bath, $\sum F_j(Q)x_j$. In the Gaussian-Markovian Fokker-Planck equation formalism, such interaction can be taken into account by the nonzero hierarchy elements, i.e., $W^{(n)}(P, R; t) \neq 0$.[17,18] By integrating the equation of motion from time $t = -t_i$ to $t = 0$, the density matrix comes to the "true" equilibrium state described by the full set of hierarchy elements $W^{(n)}(P, R; t = 0)$, if we chose $|t_i|$ sufficiently large compared to the characteristic time of the system. In the simulation, we set $|t_i| > 1/\zeta$ for $\gamma \ll \omega_0$. To evaluate the response function, we used the calculated full set of hierarchy elements $W^{(n)}(P, R; t = 0)$ as the "true" initial condition.

The simulations are performed for a harmonic mode with the frequency $\omega_0 = 38.7\,\mathrm{cm}^{-1}$ ($1/\omega_0 = 861\,\mathrm{fs}$).[25] Since we have studied the temperature effects in paper I for Gaussian-white noise, we here fixed the temperature at $T = 300\,\mathrm{K}$ and concentrate on the effect of the finite correlation time of the noise. We consider three cases of the inverse correlation time $\gamma = 0.1\omega_0$, ω_0, and $10\omega_0$ for the different coupling strengths $\zeta' = 0.01\omega_0$, $0.1\omega_0$, and $0.5\omega_0$, where we set $\zeta' = \hbar\zeta_{SL}/M\omega_0^2$. The nonlinear polarizability α_2 is chosen to be very small, i.e. $\alpha_2/\alpha_1 = 0.01$.

The kinetic equations were integrated numerically using the second order Runge-Kutta method for finite difference expressions of the momentum and the coordinate space. The size of the mesh was chosen to be 220×80 in the mesh range $-11 < r < 11$ and $-15 < p < 15$ in dimensionless momentum and coordinate (*cf.* paper I). We have taken into account $2 \sim 40$ hierarchy elements for $W^{(n)}$. The time steps for the finite difference expression $\partial W/\partial t$ were between 0.001 and 0.005 fs. The accuracy of the calculations was checked by changing the mesh size and the number of terms in the hierarchy. Using the procedure to calculate multi-time correlation functions given in ref. 25, we calculated various orders of the signal.

4.1 Third-order Raman signals (first-order IR signals)

In Fig. 3, we present the imaginary part of the Fourier transformation of the third-order response function, $R^{(3)}(\omega) = \int \mathrm{d}T_1 \exp[\mathrm{i}\omega T_1] R^{(3)}(T_1)$ for different coupling strength ζ' and inverse correlation time γ. We chose the depth of the hierarchy $n = 2 \sim 6$ for Fig. 3(a), $n = 2 \sim 10$ for Fig. 3(b), and $n = 4 \sim 40$ for Fig. 3(c). For all calculations we checked that a further increase of n does not change the response function. In the LL case, $R^{(3)}(\omega)$ directly relates to the spectral distribution $J_{\mathrm{LL}}(\omega)$, but here we do not have such a relation to $J_{SL}(\omega)$. For small ζ', Fig. 3(a) the line shapes are mainly Lorentzian and similar to those of the LL model shown in Fig. 4 in Paper I. In the LL model the Lorentzian line is due to population relaxation as was discussed in the introduction. The same line shape found in Fig. 3(a) for the SL model has, however, a different origin: At low coupling the elastic system-bath interaction governed by the term $(aa^+ + a^+a)\sum(b_j + b_j^+)$ is dominant, which leads to homogeneous pure dephasing. As pointed out by Stef-

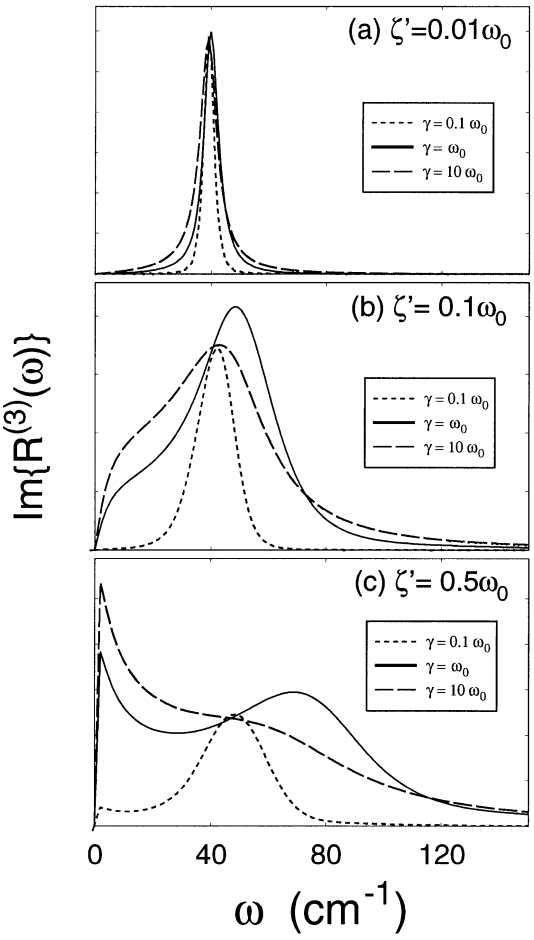

Fig. 3. The spectral density corresponds to the first-order IR or the third-order Raman response of a harmonic mode in the SL-model. We set (a) $\zeta'/\omega_0 = 0.01$, (b) $\zeta'/\omega_0 = 0.1$ and (c) $\zeta'/\omega_0 = 0.5$. In each figures, we present the results for different γ: 0.1(dashed line), 1 (solid line) and 10 (long dashed line).

fen and Duppen, ref. 13, the fifth-order 2D Raman signal is well suited to experimentally distinguish these two effects, which cannot be identified in the third-order 1D signals. The assignment to homogeneous pure dephasing will be further motivated in the next section where the 2D Raman signal in the SL model is discussed.

In Figs. 3(b) and 3(c) the third-order 1D signals are displayed for intermediate and strong coupling with $\zeta'/\omega_0 = 0.1$ and 0.5, respectively. When the correlation time of the bath fluctuations $1/\gamma$ is long, see dotted lines in Figs. 3(b) and 3(c), both spectral lines show clear Gaussian characteristics. This can be seen by noticing the similarities between these results and the results of Fig. 2(a). Also it is instructive to compare the dotted line of Fig. 3(b) to the dashed line of Fig. 3(a): while the former line has a larger full-width half maximum (FWHM) than the latter its wings are much smaller. This feature is indicative for a considerable inhomogeneous character of the underlying dynamics. The inhomogeneous line broadening can be understood intuitively by considering the main system bath interaction, which is elastic and leads to change of the effective frequency (see discussion above), and its correlation time. For a long correlation time the individual system oscillators have different frequencies, which do not change, resulting in an inhomogeneous Gaussian line shape as found in Fig. 2(a).

It should be noted that the finite size of the correlation time can be hardly extracted from the third-order signal: The differences between the pure inhomogeneous case with $\gamma = 0$ (see §3) and the finite correlation shown here is very small and only higher-order 2D techniques can be used to clearly determine the correlation time, see discussion below.

In paper I it was found that with increasing coupling strength the spectra first shift to the blue and for even larger coupling become bimodal with a second line close to zero frequency when the coupling is strong. These features, which were attributed to higher-order population relaxation proceeses due terms such as $a^2 b_j^+$, are also found for Gaussian Markovian noise, see Figs. 3(b) and 3(c). They become more pronounced as γ is increased as follows directly from the factor $\gamma^2/(\gamma^2+\omega^2)$ in eq. (8).[18] It should be noted that there is a remarkable difference compared to the GW case: The high-frequency peak shows a clear Gaussian line shape which was not found in the GW SL model of paper I. It is again indicative for the inhomogeneous character of the microscopic dynamics.

4.2 Fifth-order Raman signals (second-order IR signals)

We now present the two-dimensional (2D) signals, $I^{(5)}(T_1,T_2) = R^{(5)}(T_2,T_1)$. The laser beam configuration for this experiment was shown in Fig. 2(a) of paper I.[10] Note that we restrict our discussion to the fifth- and seventh-order off-resonant Raman spectroscopy, but the same results can be used to analyze other 2D spectroscopies such as 2D Infrared[45, 49, 50] and 2D frequency domain measurements.[39, 40, 59-61] Figure 4 shows the fifth-order 2D signals $I^{(5)}(T_1,T_2) = R^{(5)}(T_2,T_1)$ for (a) $\zeta' = 0.01\omega_0$, (b) $0.1\omega_0$, and (c) $0.5\omega_0$, for different γ (the left graphs are for intermediate modulation, $\gamma = \omega_0$, whereas the right ones are for slow modulation, $\gamma = 0.1\omega_0$). The negative part of the signal is denoted by dashed contours. Here, we omitted the case for $\gamma = 10\omega_0$, since the profiles of the signals are identical to the Gaussian-white case presented in Fig. 9 of paper I. It should be noticed that the fifth-order signal is proportional to $\alpha_1^2\alpha_2$ in this SL model. The argument[27] why lower-order contributions such as $\alpha_1^3\langle Q(t')Q(t)Q\rangle$ vanish is independent of the system-bath interaction.

In Figs. 4(a) and 4(a′) the signal is shown for small coupling strength $\zeta' = 0.01\omega_0$. As discussed above, the third-order 1D response is a Lorentzian, which resembles the response also found in the weak coupling limit of the LL model. The corresponding fifth-order responses of the LL- and SL-model, however, show some distinct differences, which are due to the different types of relaxation processes involved. In the LL model the signal decay is due to population relaxation which is effective for all quantum states. In the SL model, on the other hand, the system-bath interaction is elastic, yielding a loss of phase coherence, which affects coherent quantum states such as $|1\rangle\langle 0|$ but not population states such as $|1\rangle\langle 1|$, where $|n\rangle$ is the eigenstates of a molecular vibrational

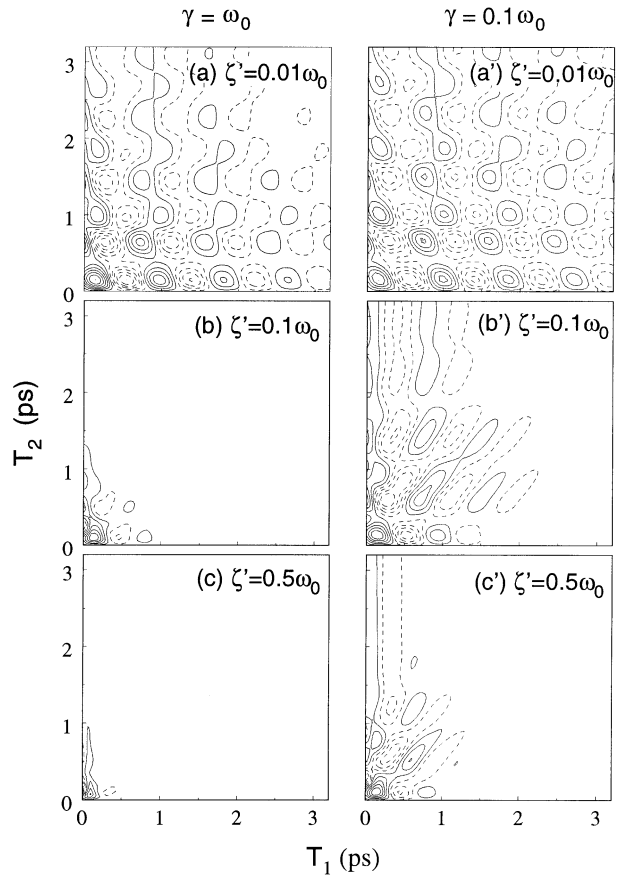

Fig. 4. Contour plot of the fifth-order Raman signal $I^{(5)}(T_1, T_2) = R^{(5)}(T_2, T_1)$ in the SL-model for (a) $\zeta'/\omega_0 = 0.01$, (b) $\zeta'/\omega_0 = 0.1$ and (c) $\zeta'/\omega_0 = 0.5$ for $\gamma = \omega_0$ and (a′) $\zeta'/\omega_0 = 0.01$, (b′) $\zeta'/\omega_0 = 0.1$ and (c′) $\zeta'/\omega_0 = 0.5$ for $\gamma = 0.1\omega_0$. Dashed contours are negative.

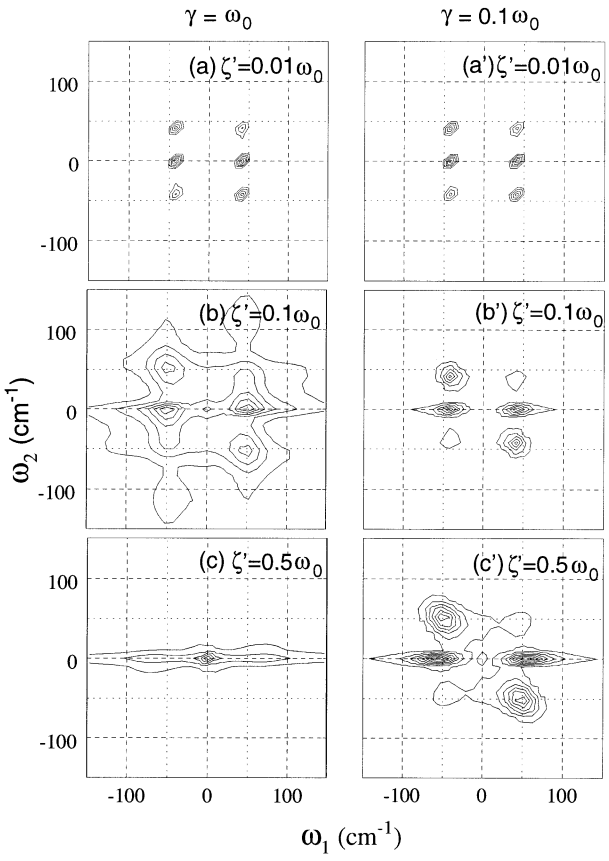

Fig. 5. Double Fourier transformation of $R^{(5)}(T_2, T_1)$ shown in Fig. 4.

mode. In impulsive fifth-order 2D Raman experiments a population state is involved in one of the Liouville path during the second propagation time. This path will not decay for pure dephasing, it is decaying only due to population relaxation.[13] Closer inspection of Figs. 4(a) and 4(a′) indeed reveals that the signal decays much slower along T_2 as compared to T_1, see in particular Fig. 4(a), and Fig. 9(a) in paper I which is identical to the case $\gamma = 10\omega_0$ in the present model. This demonstrates one of the unique features of the higher-order nonlinear experiments.

The signal for intermediate coupling is shown in Figs. 4(b) and 4(b′). For a long correlation time, i.e., a small γ, one might expect to see some indications of inhomogeneous broadening, since the third-order 1D results discussed in the previous section showed a partly Gaussian line shape. As discussed in §3 the inhomogeneity should lead to an echo feature along the diagonal at $T_1 = T_2$, see also the seminal paper by Tanimura and Mukamel, ref. 21. Indeed such a feature is clearly observed in Fig. 4(b′) while it is absent in Fig. 4(b). When the correlation time is of the order of one oscillation period (Fig. 4(b)) the system memory vanishes before an echo can be formed. This effect is further amplified by the increasing effective coupling strength with increasing γ, see discussion in the previous section, which leads to a very rapid over-all decay of the signal.

When comparing the result for a finite correlation time of 10 oscillation periods (Fig. 4(b′)) to the pure inhomogeneous limit (Fig. 2(b)) one immediately notices a remarkable difference which one could not expect by inspecting the almost identical third-order 1D spectra of Figs. 3(a) and 2(a), both dotted: In the case of a finite correlation time the echo feature along $T_1 = T_2$ decays after a few oscillation periods while it does not decay at all in the pure inhomogeneous limit of Fig. 2(b). This effect is an analogous to the effect first discussed by Loring and Mukamel[12] for a seventh-order 2D Raman process in a stochastic system. By performing a fifth-order 2D Raman experiment it is thus possible to clearly determine the correlation time of the bath fluctuations experimentally, while this is hardly possible in third-order 1D Raman experiments. In the analysis of experimental data the size of the higher-order polarizability derivatives α_2, α_3 etc. and the shape of the (inter)molecular potential are not well known, which makes the interpretation of the data quite complicated. The simultaneous analysis of various experiments such as, *e.g.*, 1D Raman, fifth- and seventh-order 2D Raman, seventh-order 3D Raman, their IR analoguous and mixtures of IR and Raman techniques will be required to fully map the interactions and dynamics. This establishes yet another unique feature of 2D spectroscopy.

In Fig. 5, the absolute value of the double Fourier transformation of the signals, $R^{(5)}(\omega_1, \omega_2) =$

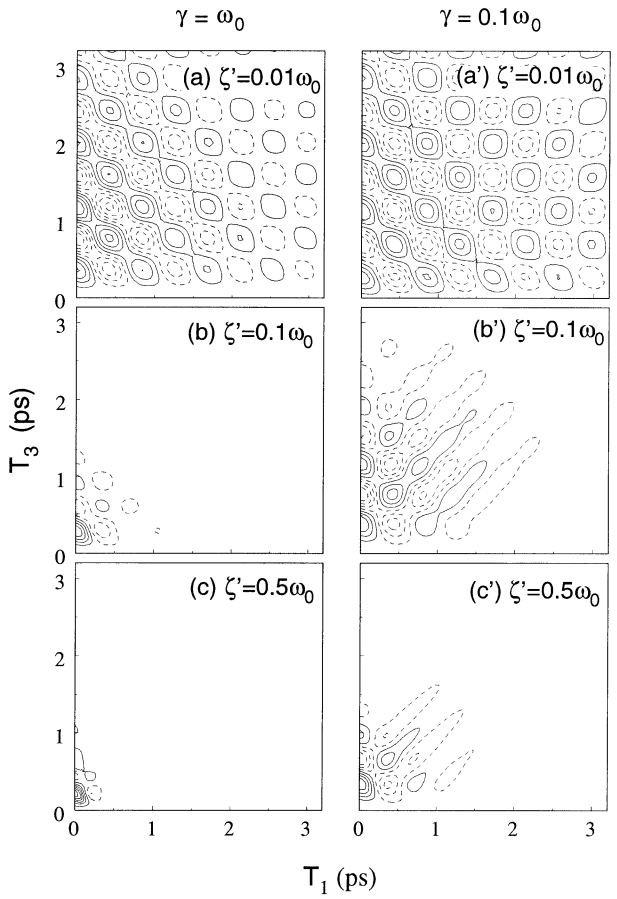

Fig. 6. Contour plot of the seventh-order Raman signal $I^{(7)}(T_1, T_3) = R^{(7)}(T_3, 0, T_1)$ in the SL-model. The order of figures are the same as Fig. 4. Dashed contours are negative.

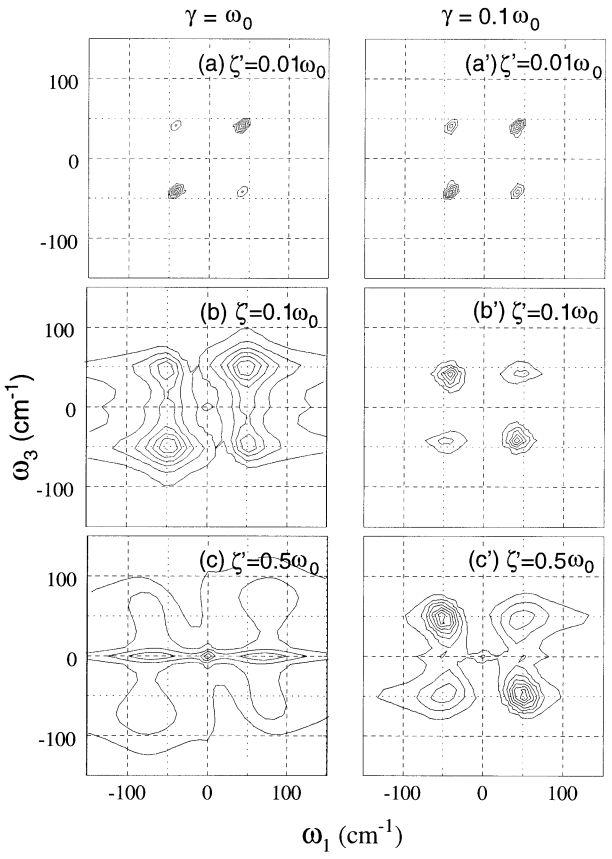

Fig. 7. Double Fourier transformation of $R^{(7)}(T_3, 0, T_1)$ shown in Fig. 6.

$|\int \mathrm{d}T_1 \int \mathrm{d}T_2 \exp[\mathrm{i}\omega_1 T_1 + \mathrm{i}\omega_2 T_2] R^{(5)}(T_2, T_1)|$ is given for the data of Fig. 4. These spectra should be compared with various two-dimensional frequency domain experiments proposed in literature.[39-46, 59-61] For large ζ', we observed peak shifts to the blue as was discussed in §4.1. The inhomogeneous dynamics observed in Figs. 4(b′) and 4(c′) can be seen also in frequency domain: The peaks at $\omega_1 = -\omega_2$ are much stronger than those at $\omega_1 = \omega_2$ as was found also in Fig. 2(b′) for the pure inhomogeneous case. The finite correlation time shows up here in the shape of the peaks at $\omega_1 = -\omega_2$, which is distinctly different from those in Fig. 2(b′). The "length" of the peak is shorter and the "width" is larger for a finite correlation time due to the smaller static and larger dynamic contribution to the line shape. For an almost homogeneous system, see Figs. 5(a) and 5(a′), the peak shapes and heights are all similar.

4.3 Seventh-order Raman signals (third-order IR signals)

In this section we discuss the seventh-order 2D Raman response signal $I^{(7)}(T_1, T_3) = R^{(7)}(T_3, 0, T_1)$ for the laser configuration shown in Fig. 2(b) of paper I. Analogously to Fig. 4, the negative signal is depicted by dashed contours. The results obtained by our quantum Fokker-Planck approach displayed in Fig. 6 should be compared with seventh-order Raman echo experiments[12, 47, 48] or third-order IR echo experiments.[49, 50]

As was discussed by Fourkas and coworkers[67] the seventh-order 2D Raman signal is proportional to $\alpha_1^2\alpha_2^2$ in the LL model since the lower-order contribution proportional to α_1^4 vanishes due to destructive interference of the Liouville space pathways involved. In paper I it was shown that this does not longer hold for the SL model and Gaussian white noise, where effective level dependent damping destroys the perfect interference. The same holds for Gaussian Markovian noise investigated here.

In the fast modulation limit illustrated in Figs. 6(a)–6(c), the system can be regarded as an ensemble of homogeneously distributed oscillators (Fig. 1(a)) and the signals exhibit very similar profiles as in Fig. 12 of paper I. For $\gamma = 0.1\omega_0$ the inhomogeneous character of the microscopic dynamics is expected to be clearly present, *cf.* discussion of the corresponding fifth-order 2D Raman response in the previous section. Indeed for large ζ' and small γ (Figs. 6(b′) and 6(c′)) a clear echo response is predicted along the diagonal $T_1 = T_3$. This is a remarkable difference compared to the inhomogeneous limit of the LL model discussed in §3 where the echo peak is found at $T_1 = 2T_3$.

The different position of the two echo peaks can be understood by considering the Liouville space path ways involved. In the LL model the α_2 term must be included to generate a signal at all, *cf.* the discussion above. This term, which corresponds to two quantum transitions, i.e.,

overtone transitions, is involved twice in each Liouville space pathway in the LL model. In a typical path the system is in a one quantum coherence during the first propagation time and a two quantum coherence during the third propagation time, *e.g.*, $|0\rangle\langle 1|$ during T_1 and $|2\rangle\langle 0|$ during T_3. In this case $T_1 = 2T_3$ has to hold to compensate for the inhomogeneous dephasing during T_1. In the SL model, where the generation of the signal relies on the level dependence of the decay mechanism, all Liouville space pathways involve only one quantum transitions. Since the system is in a one quantum coherence during both propagation times, *e.g.*, $|0\rangle\langle 1|$ during T_1 and $|1\rangle\langle 0|$ during T_3, one can immediately see that $T_1 = T_3$ has to hold for the echo peak.

Analogously to the fifth-order 2D Raman signal discussed above the decay of the echo signal in the SL model for GM noise depends on the correlation time of the fluctuations. As shown in Figs. 6(b′) and 6(c′) the echo signal along $T_1 = T_3$ decays within a few periods while it does not decay in the pure inhomogeneous limit shown in Fig. 2(c). Thus we demonstrated that also the seventh-order response is a sensitive way to measure the correlation time of the bath fluctuations.

Figure 7 illustrates the same result but in the frequency domain ($R^{(7)}(\omega_1, \omega_3) = |\int \mathrm{d}T_1 \int \mathrm{d}T_3 \exp[\mathrm{i}\omega_1 T_1 + \mathrm{i}\omega_3 T_3] R^{(7)}(T_3, 0, T_1)|$. The homogeneous character for $\zeta' = 0.01\omega_0$ is clearly evident also in the frequency domain representation, where the echo peaks at $\omega_1 = -\omega_3$ are very weak while the nonrephasing peaks at $\omega_1 = \omega_3$ are rather strong. As the system dynamics are more inhomogeneous the echo peaks get larger and the nonrephasing peaks get smaller, see Figs. 1(b′) and 1(c′). These graphs approach Fig. 2(c′) where the nonrephasing peaks are absent.

§5. Conclusions

In this paper, we derived the quantum Fokker-Planck equation with square-linear system-bath interaction for Gaussian-Markovian noise. This approach permits the treatment of colored noise and strong system-bath interaction. The effects of a finite correlation time of the bath fluctuations and of a large coupling strength were investigated by calculating the third-, fifth- and seventh-order Raman response. At intermediate and strong damping the third-order 1D Raman response shows clear traces of inhomogeneous broadening when the correlation time of the bath is long. Moreover, the spectra show a bimodal structure in the overdamped case, which is attributed to higher-order population relaxation as discussed in paper I.

Numerical calculations of the fifth-order 2D Raman response demonstrate that this spectroscopic technique is very sensitive to the correlation time of the bath fluctuations. When the system is partly inhomogeneously broadened an echo feature is predicted at $T_1 = T_2$, which decays on a time scale characteristic for the finite correction time. In the homogeneous limit the fifth-order 2D Raman response allows one to distinguish the effects of population relaxation and phase relaxation as was discussed in paper I and demonstrated also here.

Similar observation have been made for the seventh-order 2D Raman response, where also an echo signal is predicted at $T_1 = T_3$ while the Raman echo in the LL model is observed at $T_1 = 2T_3$. This difference could be explained in terms of the different Liouville space pathways involved. In this respect the seventh-order 2D Raman response in the SL model is quite similar to the fifth-order 2D Raman response. Analogous to the fifth-order 2D Raman response the seventh-order 2D Raman response is very sensitive to the finite correlation time of the bath fluctuations.

The frequency domain representation of the fifth- and seventh-order 2D Raman response allows for a clear separation of the homogeneous and inhomogeneous contributions to the total response. The shape of the 2D echo peak is a measure for both the width of the static distribution of frequencies and for the homogeneous line broadening processes. A second measure is the relative amplitude of the echo peak height with respect to the nonrephasing peak. In the inhomogeneous limit the latter is absent while it is larger than the previous peak in the homogenous limit.

In this paper, we investigate the LL and SL interaction separately, but realistic systems may have both interactions. To simulate experiments, it is also necessary to consider multi vibrational modes. Simple generalization of the present study allows us to analyze such problems. In this paper, we restricted our study to the harmonic model, but the equation of motion presented here can be applied to any potential system, such as a double well potential system for chemical reactions[17, 18] and a displaced oscillators system for nonadiabatic electronic transition.[19, 20, 68, 69] Generalizations for such directions are left for future studies.

Acknowledgments

The investigations were supported by the Grand-in-Aid on Priority Area of "Chemical Reaction Dynamics in Condensed Phases" (10206210), the Grand-in-Aid for Scientific research (B) (12440171), Shimazu Science Foundation, and by the Netherlands Foundations for Chemical Research (SON) and Physical Research (FOM) with financial aid from the Netherlands Organization for the Advancement of Science (NWO). One of us (T.S.) wants to thank the Van Dierendonck foundation of the Dutch Physical Society, Section Atomic Physics and Quantumelectronics, for a travel grant.

Appendix

The derivation of the Gaussian-Markovian quantum Fokker-Planck equation with SL interaction is parallel to the LL case shown in ref. 17. The density matrix elements for the Hamiltonian (6) with $F_j(Q) = V(Q)g_j/2$ for the distribution function (8) in the high temperature approximation $\beta\hbar\gamma \ll 1$ is expressed in the path integral form as[17, 18]

$$\rho(Q, Q'; t) = \int_{-\infty}^{\infty} \mathrm{d}Q_i \int_{-\infty}^{\infty} \mathrm{d}Q_i' \int_{Q(t_i)=Q_i}^{Q(t)=Q} \mathrm{D}[Q(t)] \int_{Q'(t_i)=Q_i'}^{Q'(t)=Q'} \mathrm{D}[Q'(t)]$$

$$\times \exp\left\{\frac{\mathrm{i}}{\hbar}(S[Q]-S[Q'])\right\}\exp\left\{-\frac{1}{\hbar}\Phi[Q,Q']\right\}\rho(Q_i,Q_i';0), \tag{A·1}$$

where

$$\Phi[Q,Q'] = \int_{t_i}^{t}\mathrm{d}s\int_{t_i}^{s}\mathrm{d}u\frac{M\zeta_{SL}\gamma}{2\hbar}\mathrm{e}^{-\gamma(s-u)}\left\{[V(Q(s))-V(Q'(s))]\left[\dot{Q}(u)\frac{\partial V(Q(u))}{\partial Q(u)}+\dot{Q}'(u)\frac{\partial V(Q'(u))}{\partial Q'(u)}\right]\right.$$
$$\left.+\,i\frac{2}{\beta\hbar}[V(Q(s))-V(Q'(s))][V(Q(u))-V(Q'(u))]\right\}. \tag{A·2}$$

We introduce the hierarchy elements

$$\rho^{(n)}(Q,Q';t) = \int_{-\infty}^{\infty}\mathrm{d}Q_i\int_{-\infty}^{\infty}\mathrm{d}Q_i'\int_{Q(t_i)=Q_i}^{Q(t)=Q}\mathrm{D}[Q(t)]\int_{Q'(t_i)=Q_i'}^{Q'(t)=Q'}\mathrm{D}[Q'(t)]$$
$$\times\left\{-\mathrm{i}\frac{M\zeta_{SL}\gamma}{2}\mathrm{e}^{-\gamma t}\left[\mathrm{i}\mathrm{e}^{-\gamma t_i}(V(Q(t_i))+V(Q'(t_i)))\right.\right.$$
$$\left.\left.+\int_{t_i}^{t}\mathrm{d}u\mathrm{e}^{-\gamma u}\left(\mathrm{i}\left[\dot{Q}(u)\frac{\partial V(Q(u))}{\partial Q(u)}+\dot{Q}'(u)\frac{\partial V(Q'(u))}{\partial Q'(u)}\right]+\frac{2}{\beta\hbar}[V(Q(u))-V(Q'(u))]\right)\right]\right\}^{n}$$
$$\times\exp\left\{\frac{\mathrm{i}}{\hbar}(S[Q]-S[Q'])\right\}\exp\left\{-\frac{1}{\hbar}\Phi[Q,Q']\right\}\rho(Q_i,Q_i';0). \tag{A·3}$$

Thus, the first member $n=0$ corresponds to the density matrix (A·1). By performing the time derivative of $\rho^{(n)}(Q,Q';t)$, we have

$$\frac{\partial}{\partial t}\rho^{(n)}(Q,Q';t) = -\frac{\mathrm{i}}{\hbar}\mathcal{L}_A(Q,Q')\rho^{(n)}(Q,Q';t) - n\gamma\rho^{(n)}(Q,Q';t)$$
$$-\frac{\mathrm{i}}{\hbar}(V(Q)-V(Q'))\rho^{(n+1)}(Q,Q';t) - \frac{\mathrm{i}n}{\hbar}\Theta_F(Q,Q')\rho^{(n-1)}(Q,Q';t), \tag{A·4}$$

where

$$\Theta_F(Q,Q') = \frac{\hbar\zeta_{SL}\gamma}{2}\left[\hbar\left(\frac{\partial V(Q)}{\partial Q}\frac{\partial}{\partial Q}-\frac{\partial V(Q')}{\partial Q'}\frac{\partial}{\partial Q'}\right)+\frac{2M}{\beta\hbar}(V(Q)-V(Q'))\right]. \tag{A·5}$$

Now we chose the square interaction, $V(Q)=Q^2$. We introduce the Wigner distribution function,

$$W(P,R;t) \equiv \frac{1}{2\pi\hbar}\int_{-\infty}^{\infty}\mathrm{d}r\mathrm{e}^{\mathrm{i}Pr/\hbar}\rho(R-r/2,R+r/2;t). \tag{A·6}$$

Then the operators are expressed as

$$Q^2-Q'^2 \to -2\frac{\hbar}{i}R\frac{\partial}{\partial P},$$
$$Q\frac{\partial}{\partial Q}-Q'\frac{\partial}{\partial Q'} \to \frac{i}{\hbar}\left[2PR+\frac{\hbar^2}{2}\frac{\partial^2}{\partial P\partial R}\right],$$
$$\Theta_F(Q,Q') \to 2\mathrm{i}\hbar\zeta_{SL}\gamma\left[R\left(P+\frac{M}{\beta}\frac{\partial}{\partial P}\right)+\frac{\hbar^2}{4}\frac{\partial^2}{\partial P\partial R}\right]. \tag{A·7}$$

Thus

$$\frac{\partial}{\partial t}W^{(n)}(P,R;t) = -\mathcal{L}_S W^{(n)}(P,R;t) - n\gamma W^{(n)}(P,R;t)$$
$$+2R\frac{\partial}{\partial P}W^{(n+1)}(P,R;t) + n2\zeta_{SL}\gamma\left[R\left(P+\frac{M}{\beta}\frac{\partial}{\partial P}\right)+\frac{\hbar^2}{4}\frac{\partial^2}{\partial P\partial R}\right]W^{(n-1)}(P,R;t). \tag{A·8}$$

Here, the quantal Liouvillian is given by eq. (12) with eq. (13). As shown in ref. 17, for deep members of the hierarchy $N\gamma \gg \omega_0$ where ω_0 is the characteristic frequency of the system such as the frequency of the harmonic potential, the above hierarchy can be terminated by

$$\frac{\partial}{\partial t}W^{(N)}(P,R;t) = -(\mathcal{L}_S+N\gamma)W^{(N)}(P,R;t) + \Gamma_{SL}W^{(N)}(P,R;t)$$
$$+N2\zeta_{SL}\gamma\left[R\left(P+\frac{M}{\beta}\frac{\partial}{\partial P}\right)+\frac{\hbar^2}{4}\frac{\partial^2}{\partial P\partial R}\right]W^{(N-1)}(P,R;t), \tag{A·9}$$

where

$$\Gamma_{SL} = 4R^2\zeta_{SL}\frac{\partial}{\partial P}\left(P + \frac{M}{\beta}\frac{\partial}{\partial P}\right) + R\zeta_{SL}\hbar^2\frac{\partial^3}{\partial^2 P\partial R}. \quad \text{(A·10)}$$

If we set $N = 0$ for $N\gamma \gg \omega_0$, we recover the square-liner Fokker-Planck equation presented in paper I.

1) P. Meystre and M. Srgent III: *Elements of Quantum Optics*, 2nd edition (Springer-Verlag, 1991).
2) S. Mukamel: *Principles of Nonlinear Optical Spectroscopy* (Oxford University Press, Oxford, 1995).
3) J. S. Bader and B. J. Berne: J. Chem. Phys. **100** (1994) 8359.
4) R. Kubo, M. Toda and N. Hashitsume: *Statistical Physics*, Vol. 2 (Springer, Berlin, 1985).
5) A. J. Leggett, S. Chakravarty, A. T. Dorsey, M. P. A. Fisher, A. Garg and Z. Zwerger: Rev. Mod. Phys. **59** (1987) 1.
6) B. R. Mollow and M. M. Miller: Ann. Phys. **52** (1969) 464.
7) Y. Tanimura and R. Kubo: J. Phys. Soc. Jpn. **58** (1989) 101.
8) Y. Tanimura and R. Kubo: J. Phys. Soc. Jpn. **58** (1989) 1199.
9) R. Kubo: *Stochastic Processes in Chemical Physics*, ed. K. Shuler (Wiley, New York, 1969) p. 101.
10) T. Steffen and Y. Tanimura: J. Phys. Soc. Jpn. **69** (2000) 3115.
11) E. T. J. Nibbering, K. Duppen and D. A. Wiersma: J. Chem. Phys. **93** (1990) 5477.
12) R. F. Loring and S. Mukamel: J. Chem. Phys. **83** (1985) 2116.
13) T. Steffen and K. Duppen: Chem. Phys. **233** (1998) 267.
14) H. Grabert, P. Schramm and G.-L. Ingold: Phys. Rep. **168** (1988) 115.
15) K. Okumura and Y. Tanimura: Phys. Rev. E **56** (1997) 2747.
16) M. Shiga and S. Okazaki: J. Chem. Phys. **111** (1999) 5390; Errata J. Chem. Phys. **113** (2000) 6451.
17) Y. Tanimura and P. G. Wolynes: Phys. Rev. A **43** (1991) 4131.
18) Y. Tanimura and P. G. Wolynes: J. Chem. Phys. **96** (1992) 8485.
19) Y. Tanimura and Y. Maruyama: J. Chem. Phys. **107** (1997) 1779.
20) Y. Maruyama and Y. Tanimura: Chem. Phys. Lett. **292** (1998) 28.
21) Y. Tanimura and S. Mukamel: J. Chem. Phys. **99** (1993) 9496.
22) K. Okumura and Y. Tanimura: J. Chem. Phys. **106** (1997) 1687.
23) K. Okumura and Y. Tanimura: J. Chem. Phys. **107** (1997) 2267.
24) K. Okumura and Y. Tanimura: Chem. Phys. Lett. **277** (1997) 159.
25) Y. Tanimura: Chem. Phys. **233** (1998) 217.
26) Y. Tanimura: *Proc. Two-Dimensional Correlation Spectroscopy* (American Institute of Physics, 2000) p. 144.
27) T. Steffen, J. T. Fourkas and K. Duppen: J. Chem. Phys. **105** (1996) 7364.
28) V. Chemyak and S. Mukamel: J. Chem. Phys. **108** (1998) 5812.
29) S. Hahn, K. Park and M. Cho: J. Chem. Phys. **111** (1999) 4121.
30) K. Park, M. Cho, S. Hahn and D. Kim: J. Chem. Phys. **111** (1999) 4131.
31) K. Park and M. Cho: J. Chem. Phys. **112** (2000) 10496.
32) K. Okumura and Y. Tanimura: Chem. Phys. Lett. **278** (1997) 175.
33) R. L. Murry, J. T. Fourkas and T. Keyes: J. Chem. Phys. **109** (1998) 7913.
34) S. Saito and I. Ohmine: J. Chem. Phys. **108** (1998) 240.
35) T. Keys and J. T. Fourkas: J. Chem. Phys. **112** (2000) 287.
36) A. Ma and R. M. Stratt: Phys. Rev. Lett. **85** (2000) 1004.
37) K. Okumura, A. Tokmakoff and Y. Tanimura: J. Chem. Phys. **111** (1999) 492.
38) S. Hahn, K. Kwak and M. Cho: J. Chem. Phys. **112** (2000) 4553.
39) J. C. Kirkwood and A. C. Albrecht and D. J. Ulness: J. Chem. Phys. **111** (1999) 253.
40) J. C. Kirkwood, A. C. Albrecht, D. J. Ulness and M. J. Stimson: J. Chem. Phys. **111** (1999) 272.
41) M. Cho, D. A. Blank, J. Sung and G. R. Fleming: J. Chem. Phys. **112** (2000) 2082.
42) T. C. Jansen, J. G. Snijders and K. Duppen: J. Chem. Phys. **113** (2000) 307.
43) M. Cho, K. Okumura and Y. Tanimura: J. Chem. Phys. **108** (1998) 1326.
44) M. Cho: J. Chem. Phys. **111** (1999) 10587.
45) M. Cho: J. Chem. Phys. **111** (1999) 4140.
46) M. Cho: Phys. Rev. A **61** (2000) 023406.
47) D. Vanden Bout, L. J. Muller and M. Berg: Phys. Rev. Lett. **43** (1991) 3700.
48) R. Inaba, K. Tominaga, M. Tasumi, K. A. Nelson and K. Yoshihara: Chem. Phys. Lett. **211** (1993) 183.
49) A. Tokmakoff, A. S. Jwok, R. S. Urdahl, R. S. Francis and M. D. Fayers: Chem. Phys. Lett. **234** (1995) 289.
50) P. Hamm, M. Lim, W. F. DeGrado and R. M. Hochstrasser: Proc. Natl. Acad. Sci. USA, **96** (1999) 2036.
51) K. Tominaga and K. Yoshihara: Phys. Rev. Lett. **74** (1995) 3061.
52) T. Steffen and K. Duppen: Phys. Rev. Lett. **76** (1996) 1224.
53) A. Tokmakoff and G. R. Fleming: J. Chem. Phys. **106** (1997) 2569.
54) D. A. Blank, L. J. Kaufman and G. R. Fleming: J. Chem. Phys. **111** (1999) 3105.
55) V. Astinov, K. Kubarych, C. J. Milne and R. J. D. Miller: Opt. Lett. **25** (2000) 853.
56) V. Astinov, K. Kubarych, C. J. Milne and R. J. D. Miller: Chem. Phys. Lett. **327** (2000) 334.
57) D. A. Blank, L. J. Kaufman and G. R. Fleming: J. Chem. Phys. **113** (2000) 771.
58) O. Golonzka, N. Demirdoven and A. Tokmakoff: *Proc. Optical Society of America, 2000.*
59) W. Zhao and J. C. Wright: Phys. Rev. Lett. **83** (1999) 1950.
60) W. Zhao and J. C. Wright: J. Am. Chem. Soc. **121** (1999) 10994.
61) W. Zhao and J. C. Wright: Phys. Rev. Lett. **84** (2000) 1411.
62) H. Riskin: *The Fokker-Planck Equation*, 2nd ed. (Springer-Verlag, Berlin, 1988).
63) A. O. Caldeira and A. J. Leggett: Physica A **121** (1983) 587.
64) C. Meier and D. J. Tannor: J. Chem. Phys. **111** (1999) 3365.
65) Y. J. Yan: Phys. Rev. A **58** (1998) 2721.
66) O. Kühn, Y. Zhao, F. Shuang and Y. J. Yan: J. Chem. Phys. **112** (2000) 6104.
67) J. T. Fourkas, H. Kawashima and K. A. Nelson: J. Chem. Phys. **103** (1995) 4393.
68) Y. Tanimura and S. Mukamel: J. Chem. Phys. **101** (1994) 3049.
69) Y. Tanimura and S. Mukamel: J. Phys. Soc. Jpn. **63** (1994) 66.